International Journal of Thermal Sciences 49 (2010) 86–98

Contents lists available at ScienceDirect

International Journal of Thermal Sciences

journal homepage: www.elsevier.com/locate/ijts

Inverse estimation for unknown fouling-layer profiles with arbitrary geometries on the inner wall of a forced-convection duct

Wen-Lih Chen*, Yu-Ching Yang

Clean Energy Center, Department of Mechanical Engineering, Kun Shan University, Yung-Kang City, Tainan 710-03, Taiwan, Republic of China

ARTICLE INFO

Article history:
Received 15 November 2008
Received in revised form
1 March 2009
Accepted 12 June 2009
Available online 14 July 2009

Keywords:
Inverse problem
Fouling layer
Duct system
Conjugate gradient method

ABSTRACT

In this study, a conjugate gradient method based inverse algorithm is applied to estimate the unknown fouling-layer profile on the inner wall of a duct system using simulated temperature measurements taken on the duct wall. The temperature data obtained from the direct problem are used to simulate the exact temperature measurements. Results show that an excellent estimation on the fouling-layer profile can be obtained for the case without separation bubble. The predictive accuracy, however, slightly deteriorates when there is a separation bubble in the duct flow. The technique presented in this study can be used in a warning system to call for maintenance when the thickness of fouling exceeds a predefined criterion.

1. Introduction

Inverse methods have recently been applied to various engineering problems. A great number of applications of inverse methods are continuously being proposed for different technical fields [1–3]. Despite the ill-posed nature of inverse problems, the solutions of these problems are important for theoretical studies and measurement techniques, especially in cases where measurement is difficult, instruments for measurement are expensive, or the measurement process to directly measure certain physical quantities is complicated. Under these circumstances, a satisfactory estimated result can be easily obtained by using a numerical method and some simple instruments, for examples, using thermocouples to measure the inner wall temperatures of burners, the temperatures of cutting tool tips, and so on. Among those different engineering applications, one of the most important applications is on a heat exchanger, a crucial element found in many engineering devices. A fundamental characteristic of a heat exchanger is the phenomenon of conjugate heat transfer which involves an interaction between the conduction of the solid wall material and the convection of the fluid flowing over that wall. The problems of conjugate heat transfer are very important and have already been examined by a number of researchers [4–6]. Many other important engineering devices also involve conjugate heat transfer problems such as flows over fins. In this case, valuable design information can be obtained by simultaneously analyzing the conduction in the fin and the convection in the fluid. For conjugate heat transfer in thick-walled pipes or ducts, the boundary conditions imposed at the external surface are different from those which exist at the internal surface. In this situation, the thermal boundary conditions existing at the internal surface are not known a priori, and hence, the energy equations must be solved under the conditions of temperature and heat flux continuity.

One of the very interesting topics of inverse problems, attracting a lot of attention in recent years, is the technique of inverse geometry problem (or shape identification problem). The applications of shape identification problem have been widely used in various industrial fields, for examples, the prediction of frost thickness in refrigeration systems, the prediction of the geometry of blast furnace inner wall, the prediction of crevice and pitting in furnace wall, and the optimization of geometry [7]. In the past, there have been many researchers devoted to the study of inverse geometry problems using a variety of numerical methods. Huang and Chen [8] developed a modified model to estimate the outer boundary configurations of a multiple region domain without confining the search directions. Park and Shin applied the coordinate transformation technique with the adjoint variable method to a shape identification problem in determining unknown boundary configuration for heat conduction systems [9] and natural convection systems [10]. Divo et al. [11] used the genetic algorithm and a singular superposition technique to detect the unknown sphere cavity in a 3D inverse geometry problem. Kwag et al. [12]

* Corresponding author.
E-mail address: wlchen@mail.ksu.edu.tw (W.-L. Chen).

1290-0729/$ – see front matter © 2009 Elsevier Masson SAS. All rights reserved.
doi:10.1016/j.ijthermalsci.2009.06.005

Nomenclature

$H1$	the height of the inner wall in the duct (m)
H_2	the height of the outer wall in the duct (m)
h	convection heat transfer coefficient ($W\,m^{-2}\,K^{-1}$)
J	functional
J'	gradient of functional
k	thermal conductivity ($W\,m^{-1}\,K^{-1}$)
L	length of the duct (m)
M	total number of measuring positions
p	direction of descent
T	temperature (K)
T_{in}	inlet temperature (K)
T_∞	ambient temperature (K)
u	fluid velocity in the x-direction ($m\,s^{-1}$)
v	fluid velocity in the y-direction ($m\,s^{-1}$)
x	spatial coordinate (m)
Y	measurement temperature (K)
y	spatial coordinate (m)
Δ	small variation quality
α	thermal diffusivity ($m^2\,s^{-1}$)
β	step size
γ	conjugate coefficient
η	very small value
λ	variable used in adjoint problem
ν	fluid kinematic viscosity $\nu = \mu/\rho$ ($m^2\,s^{-1}$)

Superscripts

K	iterative number

Subscripts

$s1$	for fouling layer
$s2$	for duct wall material
f	fluid
s	solid

followed a new algorithm to estimate the phase front motion of ice in a thermal storage system. Recently, Su and Chen [13] utilized the reversed matrix method with both the linear least-squares error method and the concept of virtual area for a shape identification problem to identify the geometry of inner wall in a furnace. Among those studies, it can be noted that there have been only very few on shape identification problems involving conjugate heat transfer which is commonly encountered in heat exchanger problems.

The performance of a heat exchanger usually deteriorates with time as a result of the accumulation of deposits on heat transfer surfaces. The layer of deposit (fouling) represents additional thermal resistance to heat transfer and causes the heat transfer rate of the heat exchanger to drop. In addition, the fouling could narrow the flow channel and result in an increase in pumping power, which in turn consumes more energy. Since fouling is often formed on the inner wall of a heat exchanger duct, it is difficult to obtain the exact configuration of the fouling layer, especially if the duct is very long. The objective of the present inverse geometry problem is to estimate the unknown irregular fouling profile on the inner wall of a duct system, which involves conjugate heat transfer, based on the simulated temperature measurements taken within the duct wall. This technique can be used in a warning system to call for maintenance when the thickness of fouling exceeds a pre-defined criterion. In the analysis, we assume the variation in the slopes of the fouling-layer profile is large, thus the duct flow will never be fully developed, and there is a possibility of forming some localized separation bubbles. Therefore, the flow field cannot be specified but needs to be solved by the Navier-Stokes equations, which have to be incorporated into the inverse procedure. In this, the Navier-Stokes equations are coupled with the inverse algorithm through the perturbation of fouling-layer profile. That is, as the fouling-layer profile is changed after an inverse iteration, a new flow field needs to be solved by the Navier-Stokes equations because the boundary of the flow domain also changed. Then the updated flow field affects the temperature distributions both in solid and fluid materials via the mechanism of conjugate heat transfer, hence altering the course of the inverse algorithm and, in turn, resulting in yet another new fouling-layer profile. The iteration cycle then goes on and on until a convergence criterion is met. Theoretically, the current inverse method is able to cope with arbitrary fouling profiles. Here, we employ the conjugate gradient method (CGM) [14–16] and the discrepancy principle [17] to the inverse geometry problem to determine the fouling-layer configuration in the duct system. The conjugate gradient method with an adjoint equation, also called Alifanov's iterative regularization method, belongs to a class of iterative regularization techniques, which mean the regularization procedure is performed during the iterative processes, thus the determination of optimal regularization conditions is not needed. On the other hand, the discrepancy principle is used to terminate the iteration process in the conjugate gradient method.

2. Analysis

2.1. Direct problem

To illustrate the methodology of developing expressions for use in determining the unknown irregular fouling profile $f(x)$, on the inner wall of a duct flow, the following steady-state heat transfer problem is considered. Fig. 1 shows a schematic representation of the considered duct flow. A duct is assumed symmetrical to the centerline. The length of the duct is L, with half heights of the inner and outer walls H_1 and H_2, respectively. The fluid temperature at the inlet is $T_{in}(y)$. After a period of operation, a layer of fouling is assumed built up on the duct's inner wall and the profile $f(x)$ of the fouling layer is assumed unknown. Then, the mathematical formulation of this steady-state forced convection heat transfer problem, covering the fouling layer, solid duct, and fluid domains, respectively, can be expressed as [18]:

Navier-Stokes equations and boundary conditions:

$$\frac{\partial u}{\partial x} + \frac{\partial v}{\partial y} = 0, \tag{1a}$$

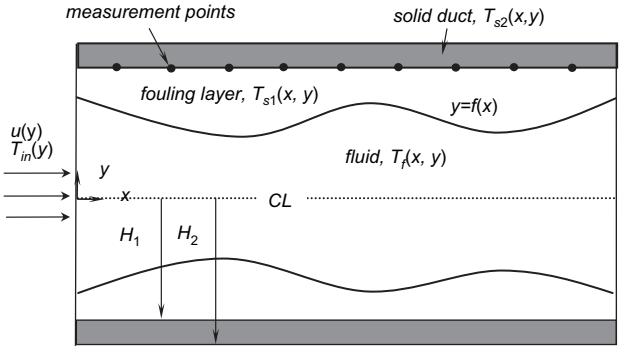

Fig. 1. Schematic of the configuration of the duct system.

$$u\frac{\partial u}{\partial x}+v\frac{\partial u}{\partial y}=-\frac{\partial p}{\partial x}+\nu\left(\frac{\partial^2 u}{\partial x^2}+\frac{\partial^2 u}{\partial y^2}\right), \tag{1b}$$

$$u\frac{\partial v}{\partial x}+v\frac{\partial v}{\partial y}=-\frac{\partial p}{\partial y}+\nu\left(\frac{\partial^2 v}{\partial x^2}+\frac{\partial^2 v}{\partial y^2}\right), \tag{1c}$$

$$u(0,y)=1.5u_{av}\left[1-\left(\frac{y}{H_1}\right)^2\right] \text{ and } v=0, \quad \text{at } x=0 \text{ and } 0\le y\le f(x), \tag{1d}$$

$$\frac{\partial u}{\partial x}=\frac{\partial v}{\partial x}=0, \quad \text{at } x=L \text{ and } 0\le y\le f(x), \tag{1e}$$

$$\frac{\partial u}{\partial y}=0 \text{ and } v=0, \quad \text{at } y=0 \text{ and } 0\le x\le L, \tag{1f}$$

$$u=v=0, \quad \text{at } y=f(x) \text{ and } 0\le x\le L. \tag{1g}$$

Energy equations and boundary conditions:
In the fluid region:

$$u\frac{\partial T_f}{\partial x}+v\frac{\partial T_f}{\partial y}=\alpha_f\left(\frac{\partial^2 T_f}{\partial x^2}+\frac{\partial^2 T_f}{\partial y^2}\right), \tag{2a}$$

$$T_f=T_{in}(y), \text{ at } x=0 \text{ and } 0\le y\le f(x), \tag{2b}$$

$$\frac{\partial T_f}{\partial x}=0, \quad \text{at } x=L \text{ and } 0\le y\le f(x), \tag{2c}$$

$$\frac{\partial T_f}{\partial y}=0, \quad \text{at } y=0 \text{ and } 0\le x\le L. \tag{2d}$$

In the fouling region:

$$\frac{\partial^2 T_{s1}}{\partial x^2}+\frac{\partial^2 T_{s1}}{\partial y^2}=0, \tag{3a}$$

$$\frac{\partial T_{s1}}{\partial x}=0, \quad \text{at } x=0 \text{ and } f(x)\le y\le H_1, \tag{3b}$$

$$\frac{\partial T_{s1}}{\partial x}=0, \quad \text{at } x=L \text{ and } f(x)\le y\le H_1. \tag{3c}$$

In the pipe wall region:

$$\frac{\partial^2 T_{s2}}{\partial x^2}+\frac{\partial^2 T_{s2}}{\partial y^2}=0, \tag{4a}$$

$$\frac{\partial T_{s2}}{\partial x}=0, \quad \text{at } x=0 \text{ and } H_1\le y\le H_2, \tag{4b}$$

$$\frac{\partial T_{s2}}{\partial x}=0, \quad \text{at } x=L \text{ and } H_1\le y\le H_2, \tag{4c}$$

$$-k_{s2}\frac{\partial T_{s2}}{\partial y}=h(T_{s2}-T_\infty), \quad \text{at } y=H_2 \text{ and } 0\le x\le L. \tag{4d}$$

At the interface between the regions of fluid and fouling:

$$T_f=T_{s1}, \quad \text{at } y=f(x) \text{ and } 0\le x\le L, \tag{5a}$$

$$k_f\frac{\partial T_f}{\partial n}=k_{s1}\frac{\partial T_{s1}}{\partial n}, \quad \text{at } y=f(x) \text{ and } 0\le x\le L. \tag{5b}$$

At the interface between the regions of fouling and pipe wall:

$$T_{s1}=T_{s2}, \quad \text{at } y=H_1 \text{ and } 0\le x\le L, \tag{6a}$$

$$k_{s1}\frac{\partial T_{s1}}{\partial n}=k_{s2}\frac{\partial T_{s2}}{\partial n}, \quad \text{at } y=H_1 \text{ and } 0\le x\le L, \tag{6b}$$

where k is the thermal conductivity, and u_{av} is the average velocity. The direct problem considered here is concerned with the determination of the medium temperature when the irregular fouling-layer configuration $f(x)$, thermal properties, and boundary conditions are known.

2.2. Inverse problem

For the inverse problem, the irregular fouling-layer configuration $f(x)$ is regarded as being unknown, while everything else in Eqs. (1)–(6) is known. In addition, temperature readings taken at some appropriate locations of the pipe wall are considered available. Referring to Fig. 1, we assume that M sensors installed along $y=y_m$ are used to record the temperature information to identify the fouling-layer configuration in the inverse calculation. The objective of the inverse analysis is to predict the unknown irregular fouling-layer profile $f(x)$ from knowledge of these temperature readings. Let the measured temperature at the measurement positions be denoted by $Y(x_i, y_m)$, $i=1\sim M$, where M represents the number of thermocouples. Then this inverse problem can be stated as follows: by utilizing the above mentioned measured temperature data $Y(x_i, y_m)$, the unknown fouling-layer configuration $f(x)$ is to be estimated over the specified domain.

The solution of the present inverse problem is to be obtained in such a way that the following functional is minimized:

$$J[f(x)]=\sum_{i=1}^{M}[T_{s2}(x_i,y_m)-Y(x_i,y_m)]^2, \tag{7}$$

where $T_{s2}(x_i, y_m)$ is the estimated (or computed) temperature at the measurement location $(x, y)=(x_i, y_m)$. These quantities are determined from the solution of the direct problem given previously by using an estimated $f^k(x)$ for the exact $f(x)$. Here $f^k(x)$ denotes the estimated quantities of $f(x)$ at the Kth iteration. In addition, in order to develop expressions for the determination of the unknown $f(x)$, a "sensitivity problem" and an "adjoint problem" are constructed as described below.

2.3. Sensitivity problem

The sensitivity problem is obtained from the original direct problem defined by Eqs. (2)–(6) in the following manner: It is assumed that when $f(x)$ undergoes a variation $\Delta f(x)$, $T(x, y)$ is perturbed by $T+\Delta T$. Then replacing in the direct problem f by $f+\Delta f$ and T by $T+\Delta T$, subtracting from the resulting expressions the direct problem, and neglecting the second-order terms, the following sensitivity problem for the sensitivity function ΔT can be obtained.

In the fluid region

$$u\frac{\partial \Delta T_f}{\partial x}+v\frac{\partial \Delta T_f}{\partial y}=\alpha_f\left(\frac{\partial^2 \Delta T_f}{\partial x^2}+\frac{\partial^2 \Delta T_f}{\partial y^2}\right), \tag{8a}$$

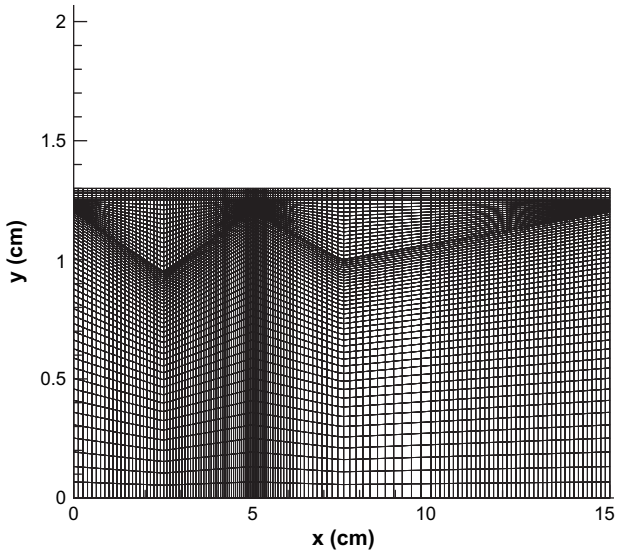

Fig. 2. The computational mesh of the direct problem.

$$\Delta T_f = 0 \quad \text{at } x = 0 \text{ and } 0 \le y \le f(x), \tag{8b}$$

$$\frac{\partial \Delta T_f}{\partial x} = 0 \quad \text{at } x = L \text{ and } 0 \le y \le f(x), \tag{8c}$$

$$\frac{\partial \Delta T_f}{\partial y} = 0, \quad \text{at } y = 0 \text{ and } 0 \le x \le L. \tag{8d}$$

In the fouling region:

$$\frac{\partial^2 \Delta T_{s1}}{\partial x^2} + \frac{\partial^2 \Delta T_{s1}}{\partial y^2} = 0, \tag{9a}$$

$$\frac{\partial \Delta T_{s1}}{\partial x} = 0 \quad \text{at } x = 0 \text{ and } f(x) \le y \le H_1, \tag{9b}$$

$$\frac{\partial \Delta T_{s1}}{\partial x} = 0 \quad \text{at } x = L \text{ and } f(x) \le y \le H_1. \tag{9c}$$

In the pipe wall region:

$$\frac{\partial^2 \Delta T_{s2}}{\partial x^2} + \frac{\partial^2 \Delta T_{s2}}{\partial y^2} = 0, \tag{10a}$$

$$\frac{\partial \Delta T_{s2}}{\partial x} = 0 \quad \text{at } x = 0 \text{ and } H_1 \le y \le H_2, \tag{10b}$$

$$\frac{\partial \Delta T_{s2}}{\partial x} = 0 \quad \text{at } x = L \text{ and } H_1 \le y \le H_2, \tag{10c}$$

$$-k_{s2}\frac{\partial \Delta T_{s2}}{\partial y} = h\Delta T_{s2}, \quad \text{at } y = H_2 \text{ and } 0 \le x \le L. \tag{10d}$$

At the interface between the regions of fluid and fouling:

$$\Delta T_f = \Delta T_{s1}, \quad \text{at } y = f(x) \text{ and } 0 \le x \le L, \tag{11a}$$

$$k_f\frac{\partial \Delta T_f}{\partial n} = k_{s1}\frac{\partial \Delta T_{s1}}{\partial n}, \quad \text{at } y = f(x) \text{ and } 0 \le x \le L. \tag{11b}$$

At the interface between the regions of fouling and pipe wall:

$$\Delta T_{s1} = \Delta T_{s2}, \text{ at } y = H_1 \text{ and } 0 \le x \le L, \tag{12a}$$

$$k_{s1}\frac{\partial \Delta T_{s1}}{\partial y} = k_{s2}\frac{\partial \Delta T_{s2}}{\partial y}, \text{ at } y = H_1 \text{ and } 0 \le x \le L. \tag{12b}$$

The sensitivity problem of Eqs. (8)–(12) can be solved by the same method as the direct problem of Eqs. (2)–(6).

2.4. Adjoint problem and gradient equation

To obtain the adjoint problem, Eqs. (2a), (3a), and (4a) are multiplied by the Lagrange multipliers (or adjoint functions) $\lambda_f(x,y)$, $\lambda_{s1}(x,y)$ and $\lambda_{s2}(x,y)$, respectively, and the resulting expressions are integrated over the correspondent space domains. Then the results are added to the right hand side of Eq. (7) to yield the following expression for the functional $J[f(x)]$:

$$J[f(x)] = \sum_{i=1}^{M}[T_{s2}(x_i,y_m) - Y(x_i,y_m)]^2 + \int_{y=0}^{f(x)}\int_{x=0}^{L} \lambda_f \cdot \left[u\cdot\frac{\partial T_f}{\partial x} + v\cdot\frac{\partial T_f}{\partial y} - \alpha_f\cdot\left(\frac{\partial^2 T_f}{\partial x^2} + \frac{\partial^2 T_f}{\partial y^2}\right)\right]dxdy + \int_{y=f(x)}^{H_1}\int_{x=0}^{L} \lambda_{s1}\cdot\left[\frac{\partial^2 T_{s1}}{\partial x^2} + \frac{\partial^2 T_{s1}}{\partial y^2}\right]dxdy + \int_{y=H_1}^{H_2}\int_{x=0}^{L} \lambda_{s2}\cdot\left[\frac{\partial^2 T_{s2}}{\partial x^2} + \frac{\partial^2 T_{s2}}{\partial y^2}\right]dxdy. \tag{13}$$

The variation ΔJ is obtained by perturbing f by Δf and T by &DeltaT; in Eq. (13). Subtracting from the resulting expression the original Eq. (13) and neglecting the second-order terms, we thus find

$$\begin{aligned}\Delta J[f(x)] = {} & \int_{y=H_1}^{H_2}\int_{x=0}^{L} 2[T_{s2}(x,y) - Y(x,y)]\Delta T_{s2}\cdot\delta(x-x_i)\cdot\delta(y-y_m)dxdy \\ & + \int_{y=0}^{f(x)}\int_{x=0}^{L} \lambda_f\cdot\left[u\frac{\partial \Delta T_f}{\partial x} + v\frac{\partial \Delta T_f}{\partial y} - \alpha_f\left(\frac{\partial^2 \Delta T_f}{\partial x^2} + \frac{\partial^2 \Delta T_f}{\partial y^2}\right)\right]dxdy + \int_{y=f(x)}^{H_1}\int_{x=0}^{L} \lambda_{s1}\cdot\left[\frac{\partial^2 \Delta T_{s1}}{\partial x^2} + \frac{\partial^2 \Delta T_{s1}}{\partial y^2}\right]dxdy \\ & + \int_{y=H_1}^{H_2}\int_{x=0}^{L} \lambda_{s2}\cdot\left[\frac{\partial^2 \Delta T_{s2}}{\partial x^2} + \frac{\partial^2 \Delta T_{s2}}{\partial y^2}\right]dxdy.\end{aligned} \tag{14}$$

where δ is the Dirac function. Utilizing the boundary conditions of the sensitivity problem, we can integrate the second to fourth double integral terms in Eq. (14) by parts. The vanishing of the integrands containing ΔT leads to the following adjoint problem for the determination of $\lambda_f(x,y)$, $\lambda_{s1}(x,y)$ and $\lambda_{s2}(x,y)$,:

In the fluid region:

$$u\frac{\partial \lambda_f}{\partial x} + v\frac{\partial \lambda_f}{\partial y} + \alpha_f\left(\frac{\partial^2 \lambda_f}{\partial x^2} + \frac{\partial^2 \lambda_f}{\partial y^2}\right) = 0, \tag{15a}$$

$$\lambda_f = 0, \quad \text{at } x = 0 \text{ and } 0 \le y \le f(x), \tag{15b}$$

$$\alpha_f\frac{\partial \lambda_f}{\partial x} + u\lambda_f = 0, \quad \text{at } x = L \text{ and } 0 \le y \le f(x), \tag{15c}$$

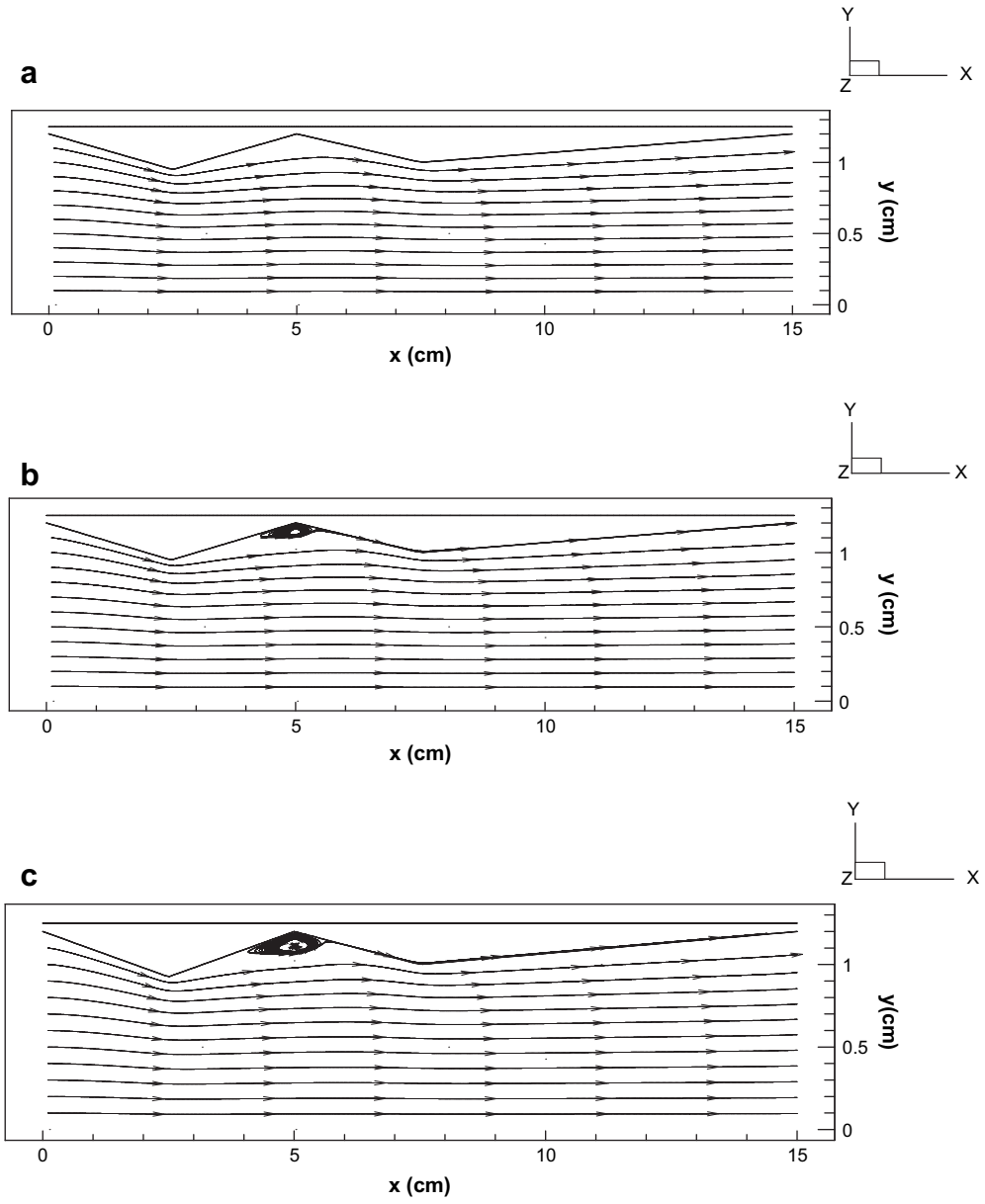

Fig. 3. Streak lines of the duct flows in the three test cases: (a) case 1, (b) case 2, and (c) case 3.

$$\frac{\partial \lambda_f}{\partial y} = 0, \quad \text{at } y = 0 \text{ and } 0 \le x \le L, \tag{15d}$$

In the fouling region:

$$\frac{\partial^2 \lambda_{s1}}{\partial x^2} + \frac{\partial^2 \lambda_{s1}}{\partial y^2} = 0\,, \tag{16a}$$

$$\frac{\partial \lambda_{s1}}{\partial x} = 0, \quad \text{at } x = 0 \text{ and } f(x) \le y \le H_1, \tag{16b}$$

$$\frac{\partial \lambda_{s1}}{\partial x} = 0 \quad \text{at } x = L \text{ and } f(x) \le y \le H_1. \tag{16c}$$

In the pipe wall region:

$$\frac{\partial^2 \lambda_{s2}}{\partial x^2} + \frac{\partial^2 \lambda_{s2}}{\partial y^2} + 2[T_{s2}(x,y) - Y(x,y)] \cdot \delta(x - x_i) \cdot \delta(y - y_m) = 0, \tag{17a}$$

$$\frac{\partial \lambda_{s2}}{\partial x} = 0 \quad \text{at } x = 0 \text{ and } H_1 \le y \le H_2, \tag{17b}$$

$$\frac{\partial \lambda_{s2}}{\partial x} = 0 \quad \text{at } x = L \text{ and } H_1 \le y \le H_2, \tag{17c}$$

$$-k_{s2}\frac{\partial \lambda_{s2}}{\partial y} = h\lambda_{s2}, \quad \text{at } y = H_2 \text{ and } 0 \le x \le L. \tag{17d}$$

At the interface between the regions of fluid and fouling:

$$k_{s1}\lambda_f = k_f\lambda_{s1}, \quad \text{at } y = f(x) \text{ and } 0 \le x \le L, \tag{18a}$$

$$k_{s1}\frac{\partial \lambda_f}{\partial n} = k_f\frac{\partial \lambda_{s1}}{\partial n}, \quad \text{at } y = f(x) \text{ and } 0 \le x \le L. \tag{18b}$$

At the interface between the regions of fouling and pipe wall:

$$k_{s2}\lambda_{s1} = k_{s1}\lambda_{s2} \quad \text{at } y = H_1 \text{ and } 0 \le x \le L, \tag{19a}$$

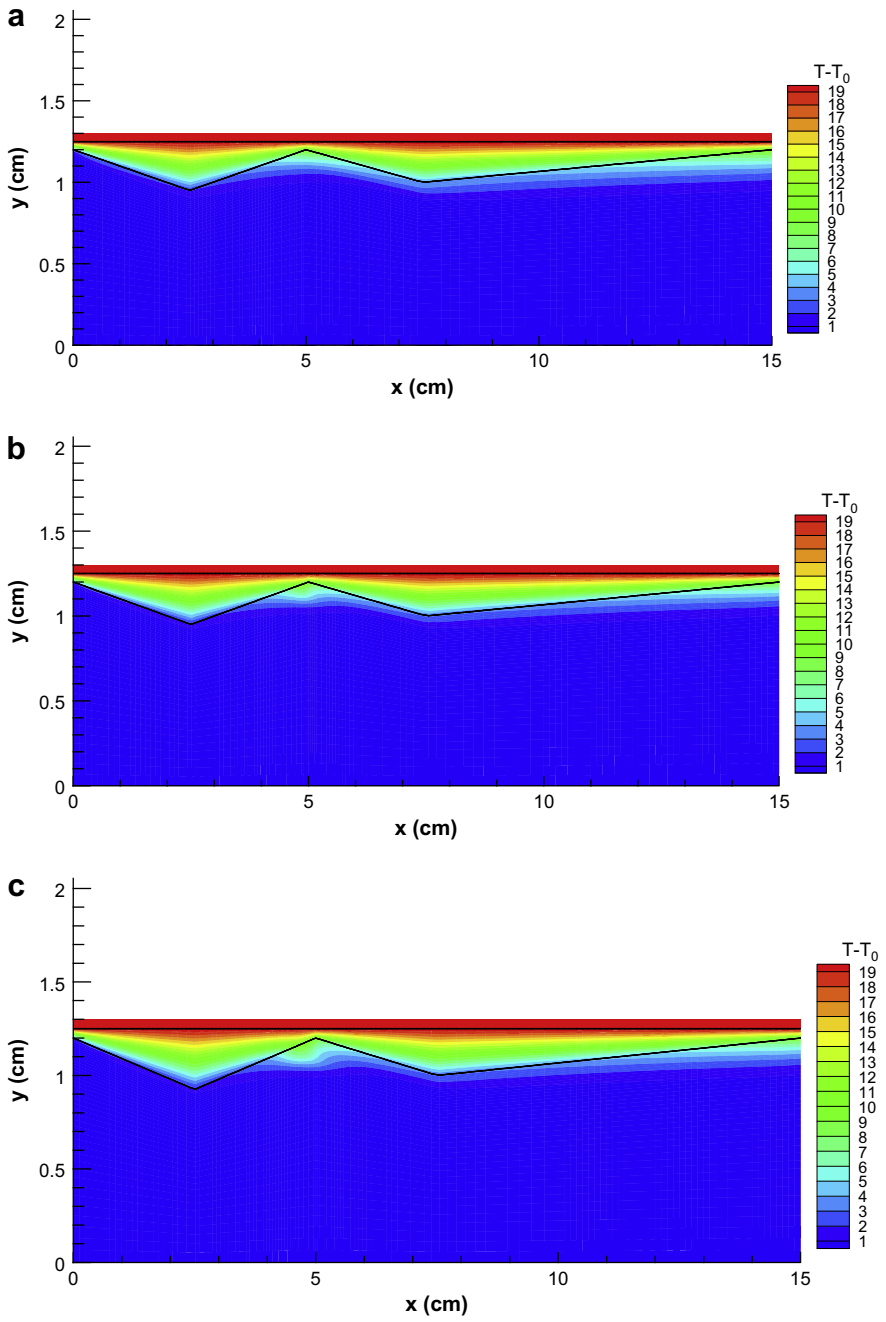

Fig. 4. Temperature contours of the three test cases: (a) case 1, (b) case 2, and (c) case 3.

$$\frac{\partial \lambda_{s1}}{\partial y} = \frac{\partial \lambda_{s2}}{\partial y}, \quad \text{at } y = H_1 \text{ and } 0 \le x \le L. \tag{19b}$$

Then the adjoint problem can be solved by the same method as the direct problem.

Finally the following integral term is left:

$$\Delta J = \int_{x=0}^{L} -\left[\frac{\partial T_{s1}}{\partial n}\frac{\partial \lambda_{s1}}{\partial n}\right]_{y=f(x)} \cdot \Delta f(x)\mathrm{d}x. \tag{20}$$

From the definition used in the reference [14], we have

$$\Delta J = \int_{x=0}^{L} J'(x)\Delta f(x)\mathrm{d}x, \tag{21}$$

where $J'(x)$ is the gradient of the functional $J[f(x)]$. A comparison of Eqs. (20) and (21) leads to the following form:

$$J'(x) = -\left[\frac{\partial T_{s1}}{\partial n}\frac{\partial \lambda_{s1}}{\partial n}\right]_{y=f(x)}. \tag{22}$$

2.5. Conjugate gradient method for minimization

Assuming the functions of $T(x,y)$, $\Delta T(x,y)$, $\lambda(x,y)$ and $J'(x)$ are available at the Kth iteration, the iteration process based on the

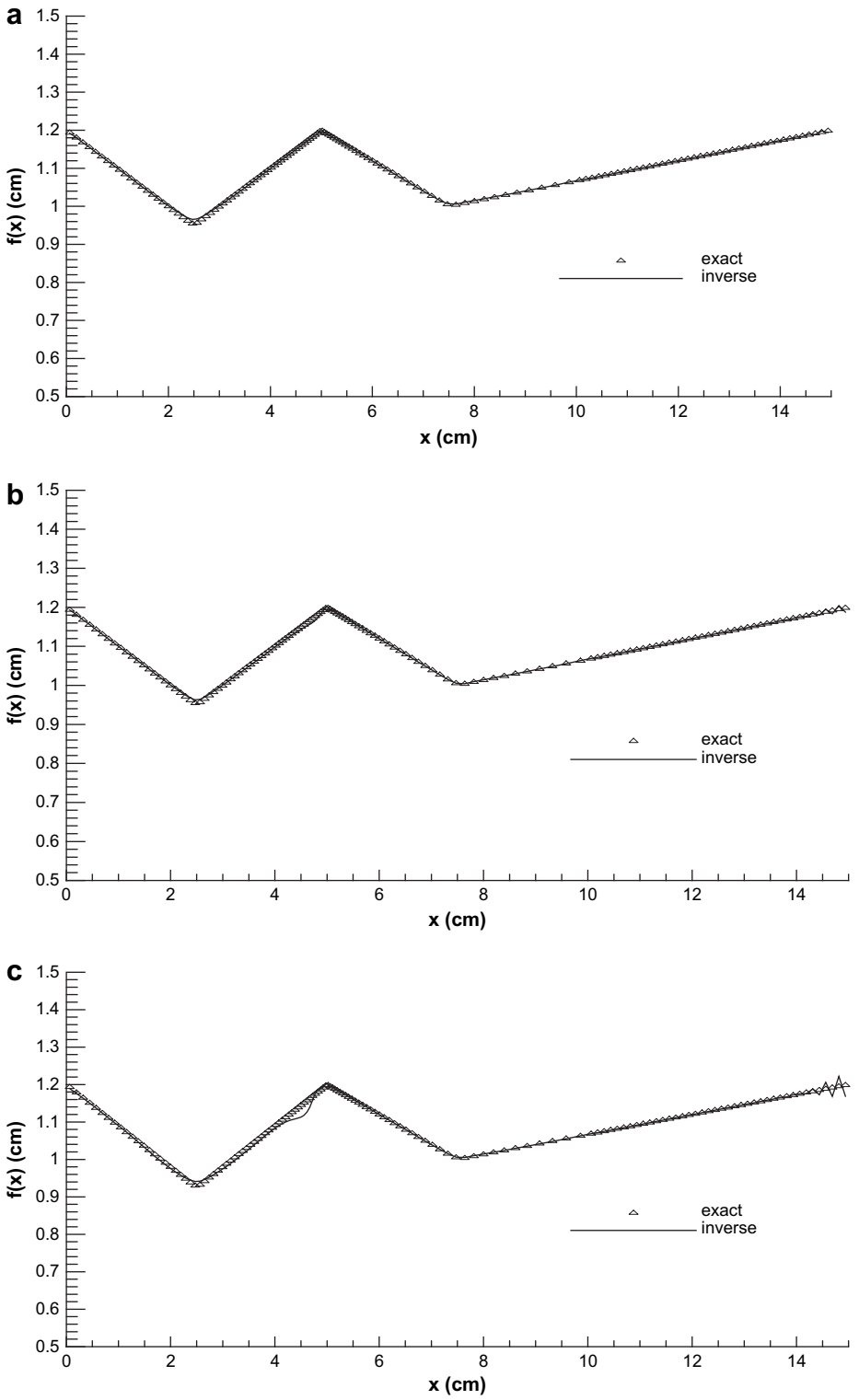

Fig. 5. Comparison of the exact and inverse fouling-layer profiles for the three cases: (a) case 1, (b) case 2, and (c) case 3.

conjugate gradient method is now used for the estimation of $f(x)$. By minimizing the above functional $J[f(x)]$, the function $f(x)$ can be evaluated at the $(K+1)$th step by

$$f^{K+1}(x) = f^{K}(x) - \beta^{K} p^{K}(x), \quad K = 0, 1, 2, \ldots, \tag{23}$$

where β^K is the search step size in going from iteration K to iteration $K+1$, and p^K is the direction of descent (i.e., search direction) given by

$$p^{K}(x) = J'^{K}(x) + \gamma^{K} p^{K-1}(x), \tag{24}$$

which is conjugation of the gradient direction $J'^{K}(x)$ at iteration K

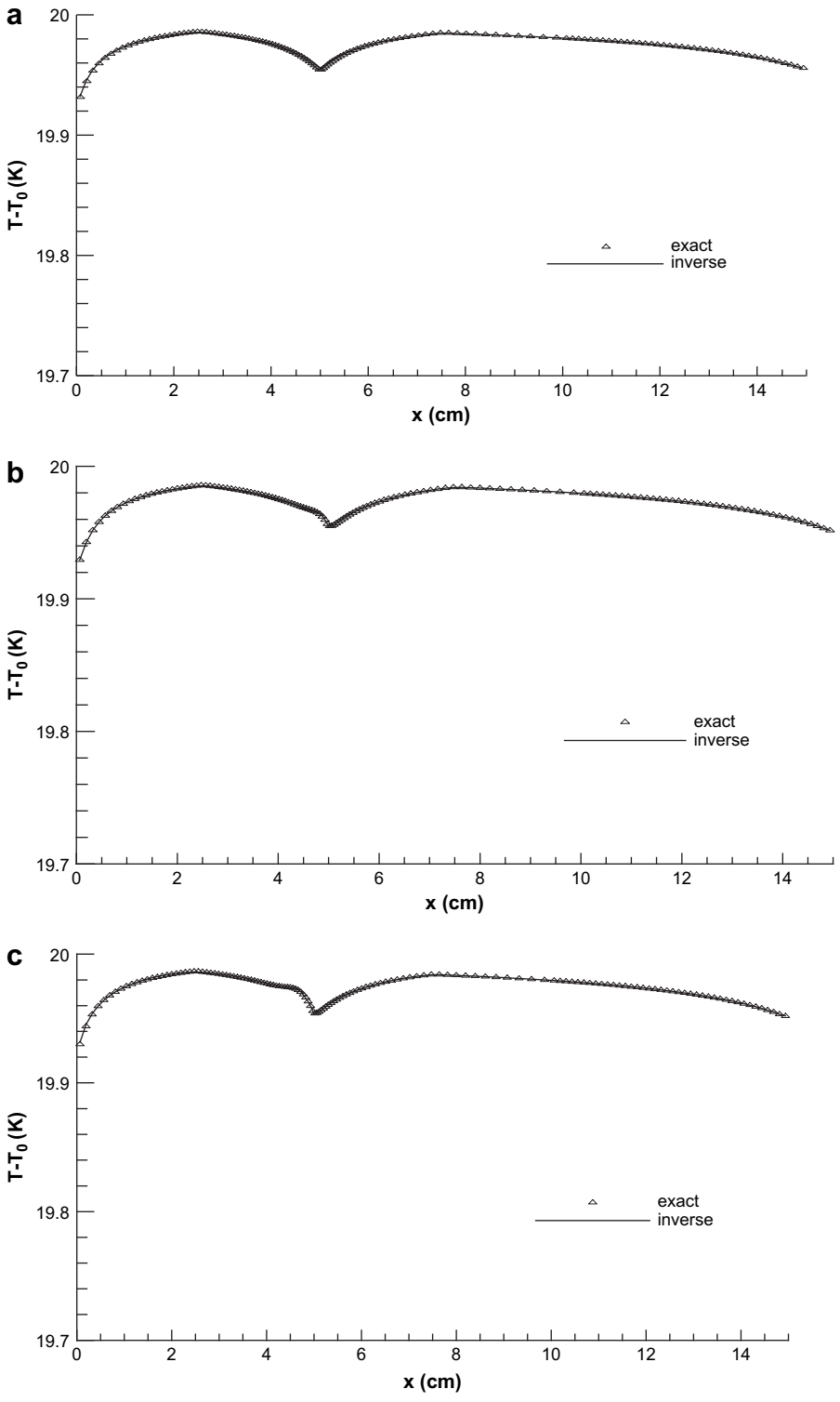

Fig. 6. Comparison of the exact and inverse measurement temperature distributions for the three cases: (a) case 1, (b) case 2, and (c) case 3.

and the direction of descent $p^{K-1}(x)$at iteration $K-1$. The conjugate coefficient γ^K is determined from

$$\gamma^K = \frac{\sum_{i=1}^{M}\left[J'^K(x)\delta(x-x_i)\right]^2}{\sum_{i=1}^{M}\left[J'^{K-1}(x)\delta(x-x_i)\right]^2} \quad \text{with } \gamma^0 = 0. \tag{25}$$

The convergence of the above iterative procedure in minimizing the functional J is proved in the reference [14]. To perform the iterations according to Eq. (23), we need to compute the step size β^K and the gradient of the functional $J'^K(x)$.

The functional $J[f^{K+1}(x)]$ for iteration $K+1$ is obtained by rewriting Eq. (7) as

$$J\left[f^{K+1}(x)\right] = \sum_{i=1}^{M}\left[T_{s2}(f^K - \beta^K p^K) - Y(x_i, y_m)\right]^2, \tag{26}$$

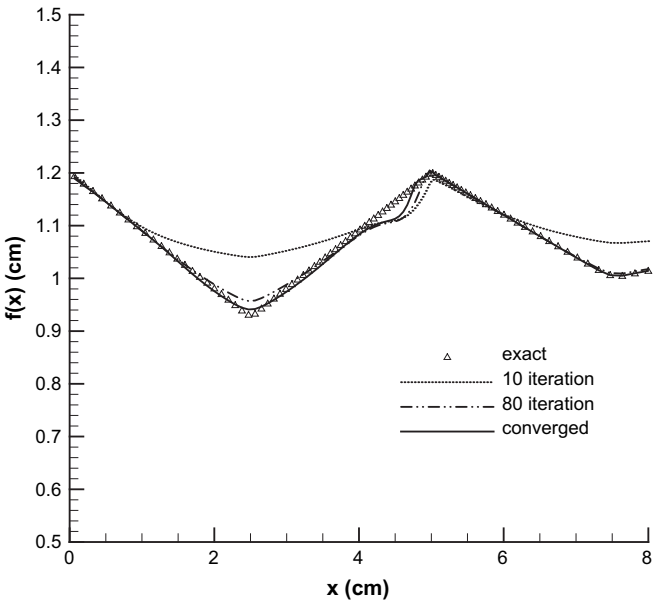

Fig. 7. Comparison of different intermediate inverse fouling-layer profiles for case 3.

where we replace f^{K+1} by the expression given by Eq. (23). If temperature T_{s2} ($f^K - \beta^K p^K$) is linearized by a Taylor expansion, Eq. (26) takes the form

$$J\left[f^{K+1}(x)\right] = \sum_{i=1}^{M}\left[T_{s2}(f^K) - \beta^K \Delta T_{s2}(p^K) - Y(x_i, y_m)\right]^2, \tag{27}$$

where $T_{s2}(f^K)$ is the solution of the direct problem at $(x, y) = (x_i, y_m)$ by using estimated $f^K(x)$ for exact $f(x)$. The sensitivity function $\Delta T_{s2}(p^K)$ is taken as the solution of Eqs. (8)–(12) at the measured position $(x, y) = (x_i, y_m)$ by letting $\Delta f(x) = p^K(x) \Delta f(x) = p^K(x)$ [19]. The search step size β^K is determined by minimizing the functional given by Eq. (27) with respect to β^K. After rearrangement, the following expression is obtained:

$$\beta^K = \frac{\sum_{i=1}^{M} \Delta T_{s2}(p^K)\left[T_{s2}\left(f^K\right) - Y(x_i, y_m)\right]}{\sum_{i=1}^{M}\left[\Delta T_{s2}(p^K)\right]^2}. \tag{28}$$

2.6. Stopping criterion

If the problem contains no measurement errors, the convergence condition for the minimization of the criterion is:

$$J\left(f^{K+1}\right) < \eta, \tag{29}$$

where η is a small specified number, can be used as the stopping criterion. However, the observed temperature data contains measurement errors; as a result, the inverse solution will tend to approach the perturbed input data, and the solution will exhibit oscillatory behavior as the number of iteration is increased [20]. Computational experience has shown that it is advisable to use the discrepancy principle [17] for terminating the iteration process in the conjugate gradient method. Assuming $T_{s2}(x_i, y_m) - Y(x_i, y_m) \cong \sigma$, the stopping criteria η by the discrepancy principle can be obtained from Eq. (7) as

$$\eta = M\sigma^2, \tag{30}$$

where σ is the standard deviation of the measurement error. Then the stopping criterion is given by Eq. (29) with η determined from Eq. (30).

2.7. Computational procedures

The computational procedure for the solution of this inverse problem may be summarized as follows:

Suppose $f^K(x)$ is available at iteration K.

Step 1 Solve the flow field given by Eqs. (1a)–(1g).
Step 2 Solve the direct problem given by Eqs. (2)–(6) for $T_f(x,y)$, $T_{s1}(x,y)$ and $T_{s2}(x,y)$, respectively.
Step 3 Examine the stopping criterion given by Eq. (29) with η given by Eq. (30). Continue if not satisfied.
Step 4 Solve the adjoint problem given by Eqs. (15)–(19) for $\lambda_f(x,y)$, $\lambda_{s1}(x,y)$ and $\lambda_{s2}(x,y)$, respectively.
Step 5 Compute the gradient of the functional $J'(x)$ from Eq. (22).
Step 6 Compute the conjugate coefficient γ^K and direction of decent $p^K(x)$ from Eqs. (25) and (24), respectively.
Step 7 Set $\Delta f(x) = -p^K(x)$ and solve the sensitivity problem given by Eqs. (8)–(12) for $\Delta T_f(x,y)$, $\Delta T_{s1}(x,y)$, and $\Delta T_{s2}(x,y)$, respectively.
Step 8 Compute the search step size β^K from Eq. (28).
Step 9 Compute the new estimation for $f^{K+1}(x)$ from Eq. (23) and return to Step 1.

3. Results and discussion

The objective of this article is to validate the present approach when used in estimating the irregular profile of the fouling layer built on a duct's internal wall accurately without prior information on the functional form of the unknown profile, a procedure called function estimation. In the present study, we assume that the material of the duct wall is steel, and the duct fluid is water. Then the material properties, geometric parameters, and thermal parameters of the system are listed as follows:

$\alpha = 1.4 \times 10^{-7}\ \mathrm{m^2\,s^{-1}}$, $\nu = 8.9 \times 10^{-7}\ \mathrm{m^2\,s^{-1}}$, $k_f = 0.5\ \mathrm{W\,m^{-1}\,K^{-1}}$,
$k_{s1} = 2.0\ \mathrm{W\,m^{-1}\,K^{-1}}$, $k_{s2} = 42.0\ \mathrm{W\,m^{-1}\,K^{-1}}$,
$H_1 = 0.0125$ m, $H_2 = 0.013$ m, $L = 0.15$ m, $T_{in}(y) = T_0 =$ constant,
$T_\infty - T_0 = 20$ K, $h = 100\ \mathrm{W\,m^{-2}\,K^{-1}}$.

The numerical procedure in this paper is based on the unstructured-mesh, fully collocated, finite-volume code, 'USTREAM' developed by the corresponding author. This is the descendent of the structured-mesh, multi-block code of 'STREAM' [21]. Since the problem is assumed to be symmetrical to the centerline of the duct, only the upper half of the domain is solved for the inverse problem. One of the numerical challenges of the current problem is that the fouling-layer profile, i.e. the solid/fluid interface, changes iteration after iteration. This affects the boundary profiles of both the fouling layer and the duct flow regions. As a result, the meshes for both regions need to be re-built after each inverse iteration. Therefore, a mesh reconstruction algorithm has been incorporated into the code to re-build the part of mesh covering the fouling layer and the duct flow (the mesh for solid duct wall is untouched). In order to test the accuracy of the present inverse analysis, we consider the simulated exact profile of the fouling layer, $f(x)$, as:

$$\begin{aligned} f(x) &= 0.012 - 0.1x\ \mathrm{m}, \quad 0 \leqq x < 0.025\ \mathrm{m};\\ f(x) &= 0.0095 - 0.1(x - 0.025)\ \mathrm{m}, \quad 0.025 \leqq x < 0.075\ \mathrm{m};\\ f(x) &= 0.012 - 0.1(x - 0.075)\ \mathrm{m}, \quad 0.075 \leqq x < 0.1\ \mathrm{m};\\ f(x) &= 0.01 + 0.05(x - 0.1)\ \mathrm{m}, \quad 0.1 \leqq x \leqq 0.15\ \mathrm{m}. \end{aligned} \tag{31}$$

As seen, Eq. (31) is a piecewise linear function which defines a W-shaped profile as shown in Fig. 2. The linear function has three

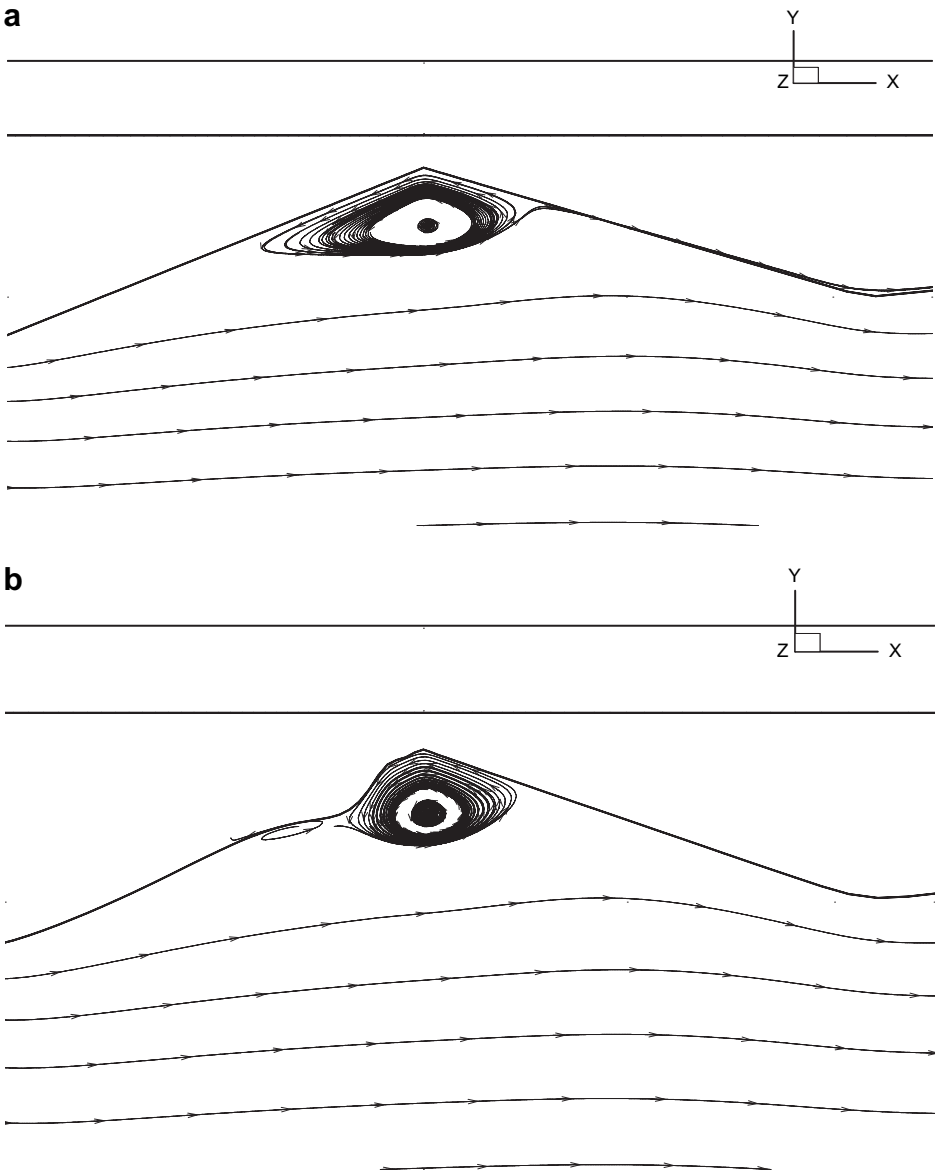

Fig. 8. Zoomed-in view of the streak lines near the separation bubble in case 3: (a) with the exact fouling-layer profile, and (b) with the inverse fouling-layer profile.

corners at $x = 0.025$, 0.05, and 0.1 m, respectively, which might be difficult for the inverse method to approximate. In addition, the profile creates two contraction and two diffusion sections within the duct and a cavity between the two peaks of the fouling layer. Under certain flow conditions, adverse pressure gradient acting on the first diffusion section can result in a separation bubble trapped within the cavity of the fouling layer, making the fluid flow more complicated. The complete mesh of the direct problem is given in Fig. 2, where the y-coordinate has been amplified 6 times to allow the profile of the fouling layer to be seen clearer. This mesh consists of 9600 cells where there are 160 and 60 cells allocated in x- and y-directions, respectively. It is also noticeable that the mesh has been compressed towards the fouling-layer/fluid interface in y-direction to increase the numerical resolution at the adjacent regions of the interface and towards the cavity in x-direction to better resolve the separation bubble if there is any. The mesh has been selected for its cell density being dense enough to return a grid-independent solution after a mesh-density test.

Here, three cases with different inlet velocities and slightly different fouling-layer geometries $f(x)$are calculated to produce different flow fields for investigating the performance of the inverse method under various flow conditions. In case 1 and case 2, the averaged inlet velocities u_{av} are set as 0.05 m s^{-1} and 0.1 m s^{-1} ($Re = 1000$ and 2000), respectively. In case 3, the averaged inlet velocity is the same as case 2, but the slope of the first peak in $f(x)$ (the first and the second expressions in Eq. (31)) is slightly increased to 0.11 to produce larger adverse pressure gradient at the first diffusion section. Fig. 3 shows the streak lines of the three cases. With a lower inlet velocity in case 1, the adverse pressure gradient at the first diffusion section is not large enough to provoke a separation bubble (Fig. 3(a)), and streak lines go smoothly along the fouling-layer/fluid interface. In case 2, however, the inlet velocity has been increased twice as much, and there exists a stronger adverse pressure gradient at the diffusion section which eventually results in a small separation bubble at the tip of the cavity (Fig. 3(b)). With a steeper slope of the first diffusion section in case 3, the strength of the adverse pressure is further intensified, and an even larger separation bubble is created (Fig. 3(c)). The size of the separation bubble poses a radical impact on the temperature distributions at its vicinity, which can be seen from the temperature

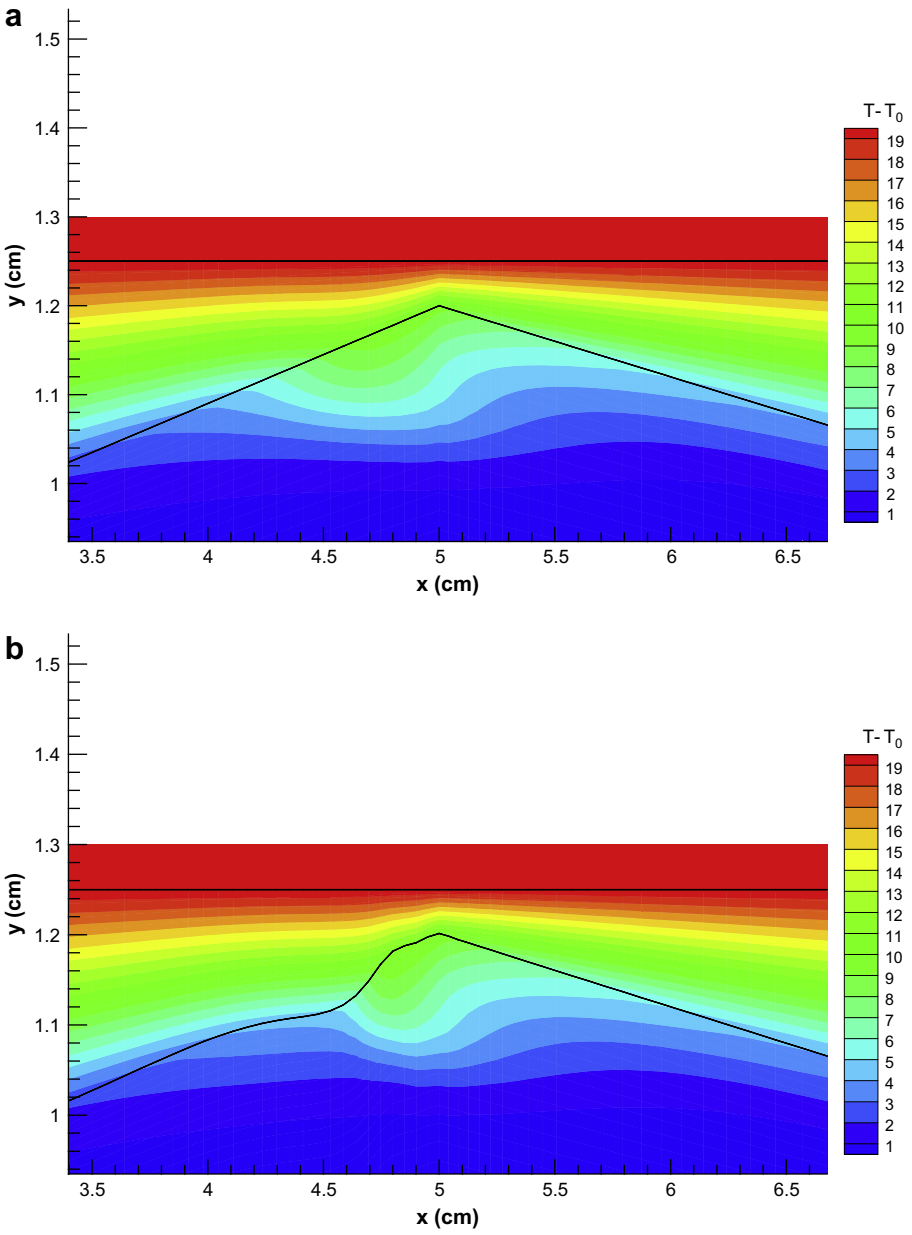

Fig. 9. Zoomed-in view of the temperature contours near the separation bubble in case 3: (a) with the exact fouling-layer profile, and (b) with the inverse fouling-layer profile.

contours shown in Fig. 4. At the diffusion sections, the adverse pressure gradient dramatically slows down the boundary-layer velocity, especially at the near-wall region, which in turn results in poor heat convection at the tip of the cavity and gives rise to a localized high-temperature region (Fig. 4(a)). The poor heat convection in this region is further worsened by the existence of a separation bubble as can be seen from Fig. 4(b) that the high-temperature region grows in size compared with Fig. 4(a). This high-temperature region is even more pronounced in Fig. 4(c) where the separation bubble is larger, suggesting that the extension of the high-temperature region seems to be in proportion to the size of the separation bubble, especially at the space occupied by the left-hand-side portion of the bubble. A very interesting phenomenon observed here is that the separation bubble poses similar effects on the temperature distribution as a thick fouling layer does. That is, they all raise the temperature at the physical space they occupy. This could be alarming and might affect the predictive accuracy of the inverse method as the same outcome can be produced by different causes; hence, the inverse algorithm might have difficulty to distinguish the effects of temperature rising at the measurement locations caused by either a thick fouling layer or a separation bubble, or a combination of the two. Therefore, the large separation bubble in case 3 presents a great challenge to the predictive accuracy of the current inverse method.

In the inverse calculation, the measurement temperature is assumed taken along the inner wall of the duct. Since we do not have a real experimental set up to measure the temperature $Y(x_i,y_m)$ in Eq. (7), we assume a real profile of the fouling layer, $f(x)$ in Eq. (31), and substitute the exact $f(x)$ into the direct problem to calculate the temperatures at the locations where the thermocouples are placed. The calculated temperatures in such way are taken as the measured temperatures. The estimated profiles for the three cases, obtained with the same initial guess of a flat profile $f^0(x) = 0.12$ m, are shown in Fig. 5. As expected, the inverse method

returns excellent agreement with the exact profile in case 1, the case without separation bubble in the flow field. For cases 2 and 3, on the other hand, the agreement deteriorates slightly, especially in case 3, only near the end of the first diffusion section where the separation bubble is located. However, the temperature distributions at the measurement locations shown in Fig. 6 indicate that the difference between the inverse and exact temperatures at the measurement locations is almost non-existence for all cases. This implies that the source term in Eq. (17a) becomes almost zero, and there is no driving force in the inverse algorithm to further correct the fouling-layer profiles for cases 2 and 3, indicating that the inverse iterations in the three cases have, in fact, all converged. To this end, it is clear that the separation bubble does undermine the predictive accuracy of the current inverse method, and the cause needs to be further investigated.

To understand why the separation bubble affects the accuracy of the inverse method, we need to examine the intermediate fouling-layer profiles during the course of the inverse iteration procedure. By zooming in the separation bubble and its adjacent region, Fig. 7 cross-plots the fouling-layer profiles after 10 and 80 iterations and the converged one from case 3. Since the initial-guess fouling profile is flat, the initial flow field is smooth without separation. Then the inverse algorithm first tried to match the measured temperatures at the measurement locations by thickening the fouling layer wherever the measured temperature is high. As a result, a thick fouling layer was developed near the tip of the cavity to mimic the effect actually caused by a separation bubble which also raises temperature at its vicinity. With the progress of the inverse iteration, the first peak of the fouling layer grows deeper into the fluid region, and the adverse pressure at the first diffusion section becomes strong enough to onset a separation bubble at the tip of the cavity. The presence of the separation bubble further raises the temperature at the region where the fouling-layer thickness has been over-predicted. The combined effect overshoots the measured temperature, which in turn signals the inverse algorithm to decrease the thickness of the fouling layer. This progressive thickness reduction can be easily observed by comparing the three inverse profiles plotted in Fig. 7. Eventually, the inverse algorithm settled down on a fouling-layer profile which is slightly thicker than the exact profile at the left-hand-side portion of the separation bubble and which gives rise to a smaller separation bubble. The zoomed-in plots of the streak lines and temperature contours near the separation bubble from the exact and inverse direct-problem solutions are given in Fig. 8 and Fig. 9, respectively. As seen in Fig. 8(b), the inverse profile actually results in two separation bubbles, a large one and the other very small one. The large separation bubble is only slightly smaller than the separation bubble created by the exact profile shown in Fig. 8(a). By further examining the corresponding temperature contours in Fig. 9(a) and Fig. 9(b), it is noticeable that there are some differences in temperature distributions at the left-hand-side portion of the separation bubble. However, there is almost no temperature difference at the measurement locations along the inner wall of the duct, which has been verified earlier by the comparison of the measurement temperature distributions shown in Fig. 6(c). This particular case is a vivid display of the ill-posed nature of an inverse problem. Fortunately, the inverse method returns highly accurate prediction for the rest of the fouling-layer profile, including the maximum and minimum thickness of the fouling layer which might be the most crucial information regarding the maintenance of the duct.

4. Conclusion

The conjugate gradient method was applied for the solution of the inverse geometry problem to determine the unknown irregular profile of fouling layer on the internal wall of a duct system with the knowledge of temperature at some measurement locations. Three cases, where the inlet velocities of the duct flow and fouling-layer geometries are different, have been conducted to examine the predictive accuracy of the inverse method under various flow conditions. According to the test results, some conclusions can be drawn as follows:

1. The current inverse method employs the Navier-Stokes equations to solve the duct flows. This implies that it could be applied to duct systems with arbitrary fouling-layer profiles.
2. Under the circumstance of no separation bubble inside the duct, the flow is simple, and the inverse method returns almost identical fouling-layer profile as the exact profile.
3. However, local separation bubbles could develop if adverse pressure gradient becomes large due to high inlet velocity or radical geometrical variations of the fouling-layer profile; and the duct flow becomes more complicated. The predictive accuracy of the inverse method slightly deteriorates at the region where a separation bubble is located.
4. The major reason contributed to the deterioration in accuracy is rooted in the ill-posed nature of an inverse problem because the inverse algorithm cannot distinguish the effects imposed by a thick fouling layer or a separation bubble on the measurement temperature, both raises temperature at their vicinities where some of the measurement points are located.
5. Despite the fouling-layer profile at the vicinity of a separation bubble is not well predicted, the inverse method returns excellent prediction for the rest of the fouling-layer profile, including the maximum and minimum thickness of the fouling layer which are of great importance regarding the scheduling of duct maintenance.

Acknowledgements

This work was supported by the National Science Council, Taiwan, Republic of China, under the grant number NSC 97-2221-E-168-039.

References

[1] P.T. Hsu, Y.H. Liu, S.G. Wang, C.K. Chen, An inverse approach for estimation of the surface heat flux distribution on a horizontal elliptical tube with laminar film condensation, Chemical Engineering Journal 85 (2002) 189–195.
[2] Y.C. Yang, S.S. Chu, W.J. Chang, Thermally induced optical effects in optical fibers by inverse methodology, Journal of Applied Physics 95 (2004) 5159–5165.
[3] H.T. Chen, X.Y. Wu, Investigation of heat transfer coefficient in two-dimensional transient inverse heat conduction problems using the hybrid inverse scheme, International Journal for Numerical Methods in Engineering 73 (2008) 107–122.
[4] E.K. Zariffeh, H.M. Soliman, A.C. Trupp, The combined effects of wall and fluid axial conduction on laminar heat transfer in circular tubes, in: Proceedings 7th International Heat Transfer Conference, Munich, Germany, vol. 4, 1982, pp. 131–136
[5] A. Campo, C. Schuler, Heat transfer in laminar flow through circular tubes accounting for two-dimensional wall conduction, International Journal of Heat and Mass Transfer 31 (1988) 2251–2259.
[6] M.A. Bernier, B.R. Baliga, Conjugate conduction and laminar mixed convection in vertical pipes for upward flow and uniform wall heat flux, Numerical Heat Transfer, Part A 21 (1992) 313–332.
[7] C.C. Chiang, S.K. Chou, Inverse geometry design problem in optimizing hull surfaces, Journal of Ship Research 42 (1998) 79–85.
[8] C.H. Huang, H.M. Chen, An inverse geometry problem of identifying growth of boundary shapes in a multiple region domain, Numerical Heat Transfer, Part A 35 (1999) 435–450.
[9] H.M. Park, H.J. Shin, Empirical reduction of modes for the shape identification problems of heat conduction systems, Computer Methods in Applied Mechanics and Engineering 192 (2003) 1893–1908.
[10] H.M. Park, H.J. Shin, Shape identification for natural convection problems using the adjoint variable method, Journal of Computational Physics 183 (2003) 198–211.

[11] E. Divo, A.J. Kassab, F. Rodriguez, An efficient singular superposition technique for cavity detection and shape optimization, Numerical Heat Transfer, Part B 46 (2004) 1–30.
[12] D.S. Kwag, I.S. Park, W.S. Kim, Inverse geometry problem of estimating the phase front motion of ice in a thermal storage system, Inverse Problems in Engineering 12 (2004) 1–15.
[13] C.R. Su, C.K. Chen, Geometry estimation of the furnace inner wall by an inverse approach, International Journal of Heat and Mass Transfer 50 (2007) 3767–3773.
[14] O.M. Alifanov, Inverse Heat Transfer Problem, Springer-Verlag, New York, 1994.
[15] B. Jin, Conjugate gradient method for the Robin inverse problem associated with the Laplace equation, International Journal for Numerical Methods in Engineering 71 (2007) 433–453.
[16] W.L. Chen, Y.C. Yang, On the inverse heat convection problem of the flow over a cascade of rectangular blades, International Journal of Heat and Mass Transfer 51 (2008) 4184–4194.
[17] O.M. Alifanov, E.A. Artyukhin, Regularized numerical solution of nonlinear inverse heat-conduction problem, Journal of Engineering Physics 29 (1975) 934–938.
[18] J. Zueco, F. Alhama, Simultaneous inverse determination of temperature-dependent thermophysical properties in fluids using the network simulation method, International Journal of Heat and Mass Transfer 50 (2007) 3234–3243.
[19] O.M. Alifanov, N.V. Kerov, Determination of external thermal load parameters by solving the two-dimensional inverse heat conduction problem, Journal of Engineering Physics 41 (1981) 581–586.
[20] O.M. Alifanov, Application of the regularization principle to the formulation of approximate solution of inverse heat conduction problem, Journal of Engineering Physics 23 (1982) 1566–1571.
[21] F.S. Lien, W.L. Chen, M.A. Leschziner, A multiblock implementation of a non-orthogonal, collocated finite volume algorithm for complex turbulent flows, International Journal for Numerical Methods in Fluids 23 (1996) 567–588.